Current Optics and Photonics
Vol. 1, No. 4, August 2017, pp. 412-420

ISSN: 2508-7266(Print) / ISSN: 2508-7274(Online)
DOI: https://doi.org/10.3807/COPP.2017.1.4.412

Label-free Noninvasive Characterization of Osteoclast Differentiation Using Raman Spectroscopy Coupled with Multivariate Analysis

Gyeong Bok Jung[1], In Soon Kang[2], Young Ju Lee[3], Dohyun Kim[4], Hun-Kuk Park[3], Gi-Ja Lee[3]*, and Chaekyun Kim[2]**

[1]Department of Physics Education, Chosun University, Gwangju 61452, Korea
[2]Department of Pharmacology, Inha University School of Medicine, Incheon 22212, Korea
[3]Department of Biomedical Engineering & Healthcare Industry Research Institute, College of Medicine, Kyung Hee University, Seoul 02447, Korea
[4]Department of Industrial and Management Engineering, Myongji University, Gyeonggi-do 17058, Korea

(Received December 22, 2016 : revised June 27, 2017 : accepted June 27, 2017)

Multinucleated bone resorptive osteoclasts differentiate from bone marrow-derived monocyte/macrophage precursor cells. During osteoclast differentiation, mononuclear pre-osteoclasts change their morphology and biochemical characteristics. In this study, Raman spectroscopy with multivariate techniques such as Principal Component Analysis (PCA) and Linear Discriminant Analysis (LDA) were used to extract biochemical information related to various cellular events during osteoclastogenesis. This technique allowed for label-free and noninvasive monitoring of differentiating cells, and clearly discriminated four different time points during osteoclast differentiation. The Raman band intensity showed significant time-dependent changes that increased up to day 4. The results of Raman spectroscopy agreed with results from atomic force microscopy (AFM) and tartrate-resistant acid phosphatase (TRAP) staining, a conventional biological assay. Under AFM, normal spindle-like mononuclear pre-osteoclasts became round and smaller at day 2 after treatment with a receptor activator of nuclear factor-κB ligand and they formed multinucleated giant cells at day 4. Thus, Raman spectroscopy, in combination with PCA-LDA, may be useful for noninvasive label-free quality assessment of cell status during osteoclast differentiation, enabling more efficient optimization of the bioprocesses.

Keywords : Osteoclast, Differentiation, Atomic force microscopy, Raman spectroscopy, Multivariate analysis
OCIS codes : (300.0300) Spectroscopy; (300.6450) Spectroscopy Raman; (170.0170) Medical optics and biotechnology; (170.1530) Cell analysis; (000.1410) Biography

I. INTRODUCTION

Most adult skeletal diseases are caused by excess osteoclast activity, leading to an imbalance in bone remodeling [1]. Excessive bone resorption is frequently observed in osteoporosis, rheumatoid arthritis, periodontal disease, cancer metastasis, and multiple myeloma, and osteoclasts play a critical role in these diseases [2, 3]. Osteoclasts are formed by the cellular fusion of bone marrow-derived mononuclear precursors and are responsible for organic bone resorption [4]. Precursor cells differentiate into mononuclear pre-osteoclasts and fuse to form multinucleated osteoclasts. Osteoclastogenesis is promoted by macrophage colony-stimulating factor (M-CSF), receptor activator of nuclear factor-κB ligand (RANKL), and osteoprotegerin. M-CSF induces expression of the RANKL receptor (RANK) and supports the survival and proliferation of osteoclast precursors [5]. RANKL stimulates the differentiation of precursors into osteoclasts by inducing expression of osteoclast-specific genes, including tartrate-resistant acid phosphatase (TRAP), cathepsin K, and calcitonin receptor [2, 6, 7].

To evaluate the differentiation stages of osteoclasts,

Corresponding author: *gjlee@khu.ac.kr, **chaekyun@inha.ac.kr
Color versions of one or more of the figures in this paper are available online.

conventional biological assays such as immune staining and western blotting are widely used [8-11]. However, these traditional methods are time-consuming, labor-intensive, and involve complex procedures that use large amounts of material and result in low product yield. Moreover, these methods cannot directly investigate the dynamics of biological molecules because cell destruction or introduction of chemical labels during measurements can alter the biological conditions. Therefore, noninvasive label-free techniques for evaluating osteoclast differentiation are needed for real-time monitoring of live cells.

Raman spectroscopy may be useful for a variety of biomedical applications because it enables observation of the dynamics of intracellular molecules in a natural environment without labeling [12-15]. Raman spectroscopy provides information regarding molecular structure, chemical composition and molecular interactions in tissues and cells. It also provides quantitative information and exhibits high sensitivity and selectivity. Intracellular information about nucleic acids, proteins and other components and their conformations can be used to identify variations in spectral shape or intensity [16-18]. Raman spectroscopy has been proposed as a technique for noninvasive label-free characterization of stem cells [19-24]. McManus *et al*. evaluated the osteogenic differentiation of human mesenchymal stem cells using Raman spectroscopy [19]. Raman spectra show dramatic changes in a region of human mesenchymal stem cells dominated by stretching phosphate groups (950-970 cm^{-1}) at 7-28 days. Notingher *et al*. used Raman spectroscopy to measure time-resolved molecular changes in intact embryonic bodies during *in vitro* cardiogenic differentiation [22]. However, osteoclast differentiation has not been evaluated by Raman spectroscopy.

Atomic force microscopy (AFM) based techniques offer advanced and elegant methods for characterizing surface properties and changes to the mechanical properties of the cell membrane [25-27]. AFM, a type of high-resolution scanning probe microscopy, is a powerful tool for imaging at the nanometer level and observing cellular ultrastructures [28, 29].

In this study, we conducted Raman spectroscopy combined with multivariate statistical techniques to investigate the biochemical characteristics at different time points during a differentiation time course of osteoclastogenesis. We also investigate the morphological characteristics of osteoclast differentiation using AFM. Furthermore, we compared conventional biological TRAP staining assays with AFM and Raman spectroscopy results.

II. MATERIALS AND METHODS

2.1. Mice

Six-week-old male C57BL/6J mice (Bar Harbor, ME, USA) were housed under pathogen-free conditions at the animal facility of Inha University. All experiments were conducted in accordance with institutional guidelines approved by the Animal Care and Use Committee of Inha University (INHA 131217-255).

2.2. Osteoclast Formation

Bone marrow cells were obtained from a single mouse. The bone marrow cells were obtained from femurs and tibias flushed with 3 mL of α -minimal essential medium (Hyclone, Logan, UT, USA) using a 22-gauge needle (BD Biosciences, Franklin Lakes, NJ, USA). The cells were pelleted by centrifugation at 600 × g for 10 min at 4°C and the red blood cells were lysed. Bone marrow cells from 6-week-old male mice were cultured overnight in α-minimal essential medium containing 10% fetal bovine serum, 100 U/mL penicillin and 100 μg/mL streptomycin. Nonadherent cells were cultured with 30 ng/mL M-CSF (Peprotech, Rocky Hill, NJ, USA) for 3 days to induce differentiation to pre-osteoclasts. Pre-osteoclasts were cultured for 4-6 days with 30 ng/mL M-CSF and 50 ng/mL RANKL (Peprotech) on either 48-well plates for light microscopy or gold-coated glass for Raman and AFM. Osteoclast formation was assessed by counting TRAP-positive cells containing more than three nuclei. All experiments were performed in triplicate and repeated at least three times.

2.3. TRAP Staining

Cells were stained using Leukocyte Acid Phosphatase Assay kits (Sigma, St Louis, MO, USA) following the manufacturer's instructions. Cells were washed with phosphate-buffered saline (PBS) and fixed with fixative solution containing citrate, acetone, and 37% formaldehyde. Fixed cells were incubated with TRAP-staining solution containing Fast Garnet GBC, sodium nitrite, naphthol AS-BI phosphoric acid, acetate, and tartrate for 1 h at 37°C in the dark. After washing with water, the cells were counterstained with hematoxylin. TRAP-positive cells containing three or more nuclei were counted under a light microscope.

2.4. AFM Measurements

Noncontact-mode AFM images were obtained using a NANOS N8 NEOS (Bruker, Billerica, MA, USA) equipped with a $42.5 \times 42.5 \times 4$ μm^3 XYZ scanner and two Zeiss optical microscopes (Epiplan 200× and 500×). To eliminate external noise, the AFM was placed on an active vibration isolation table (TS-150, Surface Imaging Systems, Herzogenrath, Germany) inside a passive vibration isolation table (Pucotech, Seoul, Korea). Cells were scanned at a resolution of 512 × 512 pixels with a scan rate of 0.7 lines/s.

2.5. Raman Spectroscopic Measurements

For Raman analysis, bone marrow cells (5×10^4) were seeded onto gold-coated glass (5 × 5 mm) and cultured for 6 days in the presence of M-CSF and RANKL. In this study, we used a gold-coated substrate to minimize spectral contributions from the glass substrate. Differentiating osteoclasts were fixed with 4% paraformaldehyde in PBS

for 20 min. After fixation, the gold-coated substrate was briefly washed with PBS and water and air-dried. Previous studies showed that formalin (and paraformaldehyde) fixation preserves lipid, phosphate, and protein components without significantly influencing the infrared (and Raman) spectrum of cells [30-32].

Raman spectra were acquired using the SENTERRA confocal Raman system (Bruker) equipped with a 785-nm diode laser source (100 mW before objective) and resolution of 3 cm^{-1}. A 100× air objective (MPLN N.A. 0.9, Olympus), which produced a laser spot size of ~1 μm was used to collect Raman signals and focus the laser on a single cell. The Raman spectra of the cell associated with auto-fluorescence background were displayed by a computer in real-time and saved for further analysis. An automated algorithm for autofluorescence background removal was applied to the measured data to extract pure sample Raman spectra. The Raman spectra of the cells were calculated as the average of ten measured samples. Baseline correction was performed using the rubber-band method, to stretch between the spectrums endpoints. All baselines corrected Raman spectra were normalized using the vector normalization method. All Raman measurements were recorded with an accumulation time of 60 s in the 600-1750 cm^{-1} range, and Raman spectral acquisition and preprocessing of preliminary data such as baseline subtraction, smoothing, normalization and spectrum analysis were carried out using OPUS software (Bruker).

2.6. Multivariate Analysis

Principal component analysis (PCA) and linear discriminant analysis (LDA) were used for statistical data analysis. For PCA and LDA, the classification toolbox for MATLAB was used. Raman spectra dataset consists of 40 observations and each 10 observations were measured on different days (i.e., days 0, 2, 4, and 6). PCA was first performed for Raman spectral data and then LDA was conducted based on the obtained PCA scores. In PCA, Raman intensities measured at 2301 frequencies (600-1750 cm^{-1}) were used as original variables and based on their linear combinations, 10 principal components were obtained. LDA generates the discriminant function based on the obtained principal components (PC) scores.

III. RESULTS AND DISCUSSION

To generate osteoclasts, bone marrow-derived pre-osteoclasts were cultured for 6 days with MCSF and RANKL. At day 4, the cells started to differentiate and form multinucleated osteoclasts (Fig. 1). Thereafter, the cell membranes became damaged and apoptotic.

Fully differentiated osteoclasts were TRAP-positive and contained more than three nuclei (Fig. 2(a)). At day 4, 237 ± 10 osteoclasts were generated, which decreased to 18 ± 8 (13.6% of day 4) at day 6 (Fig. 2(b)). This result indicates that differentiation reached a maximum at day 4 and differentiated osteoclasts began to die thereafter.

AFM is used to obtain cellular surface information, such as cellular damage because changes in cell ultrastructure and morphology after biochemical reactions or external stimuli can be detected [33-35]. We performed AFM to

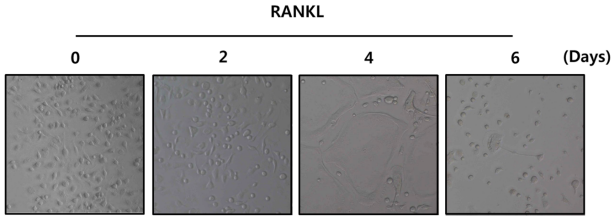

FIG. 1. RANKL-induced osteoclast differentiation. Bone marrow-derived pre-osteoclasts were differentiated on glass coverslips in the presence of 30 ng/mL M-CSF and 50 ng/mL RANKL for 6 days. Osteoclast formation was observed under the microscope (×100).

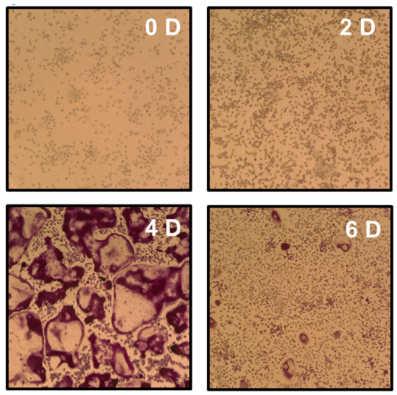

(a)

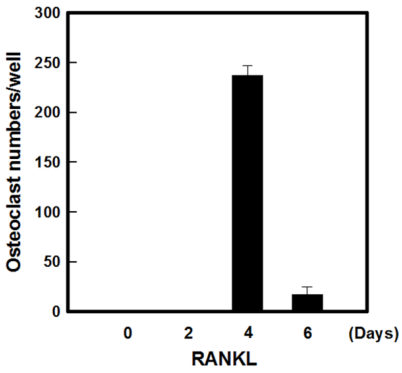

(b)

FIG. 2. Osteoclast differentiation from bone marrow-derived pre-osteoclast: (A) Bone marrow-derived pre-osteoclasts were cultured with 30 ng/mL of M-CSF and 50 ng/mL of RANKL for 6 days, and cells were stained with TRAP; (B) TRAP-positive multinuclear cells containing three or more nuclei were counted. Data were mean ± SD of two independent experiments done in triplicates.

observe morphological changes of cells during osteoclast differentiation.

Figure 3 shows representative AFM topography, line profiles and three-dimensional images of cells at 0, 2, 4 and 6 days after M-CSF and RANKL treatment. Pre-osteoclasts appeared to have a normal spindle-like shape at day 0 (Fig. 3(a)). At day 2, the cell morphology changed from spindle to small round and several cells began to gather together (Fig. 3(b)). Four days after RANKL treatment, the fusion of several cells was observed (Fig. 3(c)). These results revealed the morphological conversion from mononuclear to multinuclear cells, which is characteristic of a mature stage in osteoclast differentiation. Finally, many irregular holes appeared in the membrane surface at day 6 (Fig. 3(d)). As shown in Figs. 1 and 2, differentiation reached a maximum on day 4, after which differentiated osteoclasts began to die. This indicates that changes to the membrane surface contributed to cell death.

Raman spectroscopy allows the continuous analysis of differentiation or dynamic death events in single cells by investigating the overall molecular constitutions of individual cells within their physiological environment. A Raman peak is uniquely defined by spectral parameters including Raman shift, intensity, and full width at half maximum. These features reveal information about a specific molecular vibration. During osteoclast differentiation, intracellular information about nucleic acids, proteins and other components and their conformations can be used to identify variations in spectral shape or intensity.

Figure 4(a) shows averaged Raman spectra for undifferentiated pre-osteoclasts (0 day) and osteoclasts at days 2, 4 and 6. Cellular constituents and peak assignments for osteoclasts are shown in Table 1. The Raman spectra in Fig. 4(a) showed peaks corresponding to the molecular vibration of all cellular components including nucleic acids, proteins, lipids and carbohydrates, and were similar to previous Raman spectra for other cell types [20, 36-38]. The main changes in proteins were observed at 851, 1002, 1264, and 1656 cm^{-1}. The band at 851 cm^{-1} was assigned to tyrosine, and the sharp band at 1002 cm^{-1} corresponded to the ring stretching of phenylalanine. The broad bands at 1230-1320 and 1656 cm^{-1} represented amide III and amide I, respectively. The 1095 cm^{-1} peak represented the vibrations of phosphodioxy groups (PO_2^-) in the DNA/RNA backbones. The strong band at 1446 cm^{-1} (CH deformations) was attributed to nucleic acid, proteins and lipids. Other weaker molecular vibrations were observed at 960 and 1030 cm^{-1} (PO_4^{3-} symmetric stretch), which is associated with hydroxyapatite.

For quantitative identification, we selected specific Raman peaks corresponding to DNA/RNA, proteins, or lipids and compared changes in their spectral intensities (Fig. 4(b)). Raman spectra exhibited significant time dependence; Raman peak intensity increased up to 4 days. Four days after differentiation, an increase in the magnitude of Raman intensity for proteins was observed, specifically 1.6-fold

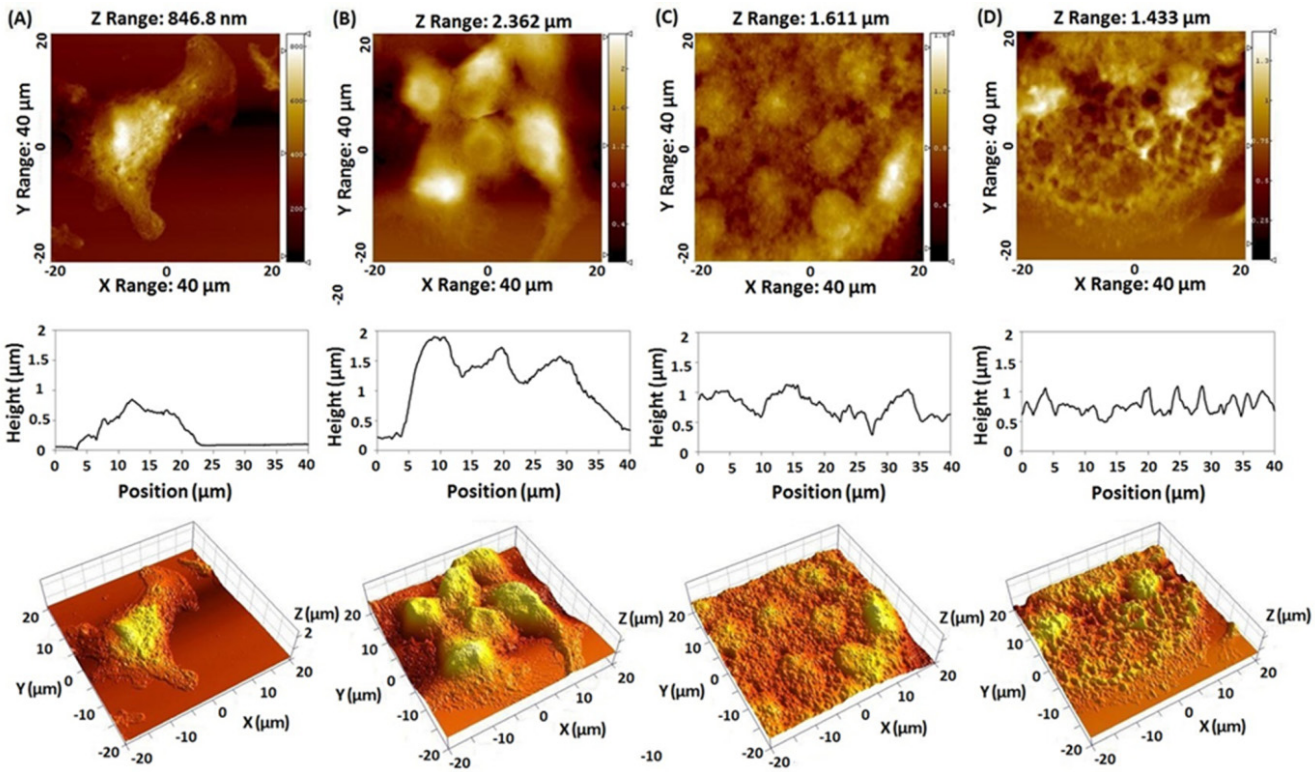

FIG. 3. Representative AFM topography, line profile, and three-dimensional images of pre-osteoclast cells for (A) 0, (B) 2, (C) 4 and (D) 6 days after RANKL treatment.

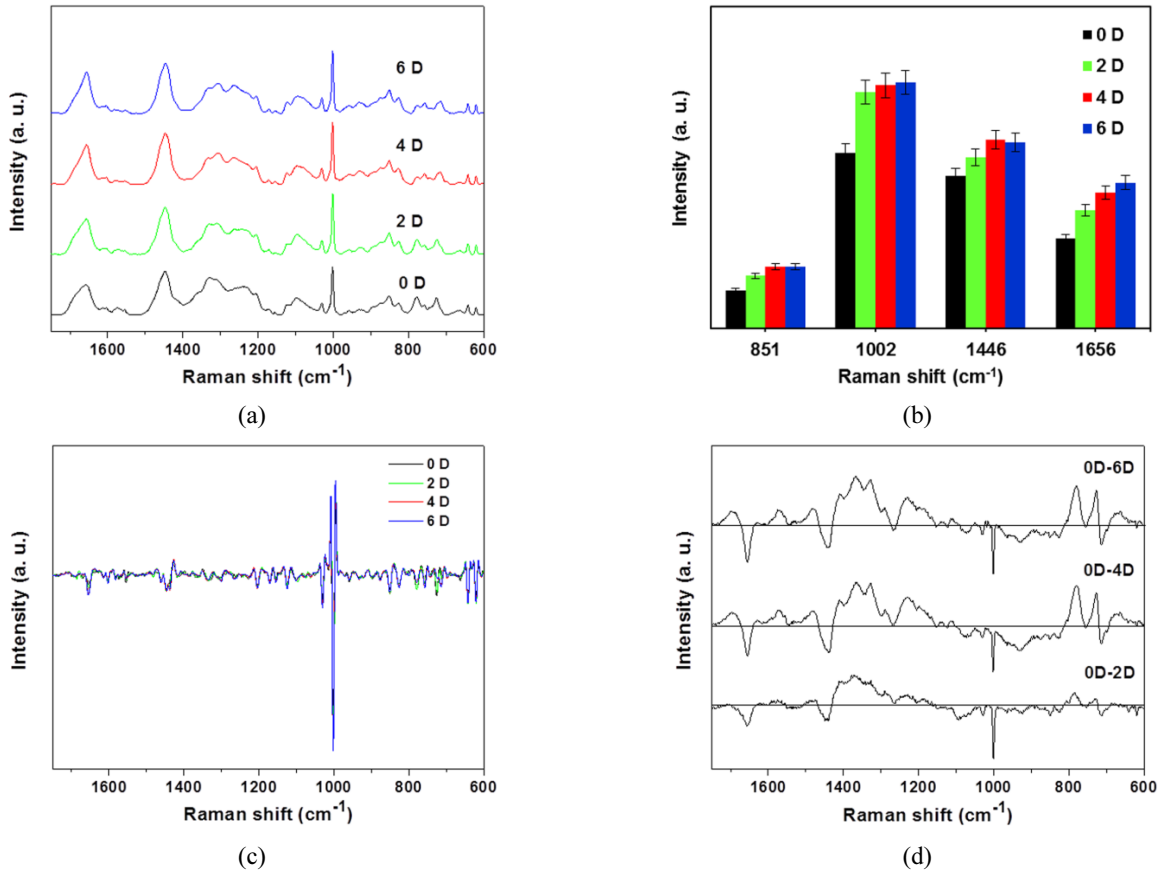

FIG. 4. (A) Time-course averaged Raman spectra, (B) Relative intensities of the Raman peak, (C) Second derivative Raman spectra, and (D) Second derivative Raman spectra difference for mononuclear pre-osteoclast (0 D) and differentiated cells for 2, 4 and 6 days (2 D, 4 D and 6 D).

TABLE 1. Peak assignment of Raman spectra for pre-osteoclasts and differentiated osteoclasts [20, 36-38]

Peak (cm^{-1})	Assignment[a]				
	DNA/RNA	Proteins	Lipids	Carbohydrates	Hydroxyapatite
621		C-C twist. Phe			
643		C-C twist. Tyr			
667	G, T				
717			$CN^{+}(CH_3)_3$ str. Choline group		
725	A				
758		Ring br. Trp			
778	U, C, T ring br.				
828	O-P-O asym. str.	Ring br. Tyr			
851		Ring br. Tyr			
877			$C\text{-}C\text{-}N^{+}$ sym. Str.	C-O-C ring	
932		C-C bk str. α-helix		C-O-C glycos	
960					PO_4^{3-} sym. str.

TABLE 1. Peak assignment of Raman spectra for pre-osteoclasts and differentiated osteoclasts [20, 36-38] (Continue)

Peak (cm^{-1})	Assignment[a]				
	DNA/RNA	Proteins	Lipids	Carbohydrates	Hydroxyapatite
1002		Sym. Ring br. Phe			
1031		C-H in-plane Phe			
1095	PO_2- str.		Chain C-C str.	C-O, C-C str.	
1124			C-C str.		
1156		C-C/ C-N str.			
1172		C-H Tyr, Phe			
1207		C-C_6H_5 str. Phe, Trp			
1237		Amide III, β-sheet			
1264		Amide III, α-helix			
1303		CH_3CH_2 twist.			
1314		CH_3CH_2 twist.			
1446	G, A	CH def	CH def	CH def	
1573	G, A				
1604		C=C Phe, Tyr			
1656		Amide I, α-helix	C=C str.		

[a]Abbreviations: A, adenine; U, uracil; G, guanine, C, dytosine; T, thymine; Phe, phenylalanine; Tyr, tyrosine; Trp, tryptophan; br, breathing; bk, backbone; def, deformation vibration; str, stretching; sym, symmetric; asym, asymmetric; tw, twist

for peak 851 cm^{-1}, 1.4-fold for 1002 cm^{-1}, 1.2-fold for 1446 cm^{-1}, and 1.5-fold for 1656 cm^{-1}. These results suggest that protein conformation increasingly changed over time, and 4 days is the optimal time period for osteoclastogenesis. Thereafter at day 6, differentiated osteoclasts began to die. Denaturation and conformational changes in proteins, and degradation of DNA are related to the cell death. These results showed good agreement with the TRAP staining results obtained using conventional biological assays as described in the previous section.

We also performed second derivative transformation of the Raman spectra. The second-derivative transformations can reduce replicate variability, correct baseline shift, and resolve overlapping bands [39]. The second derivatives of the Raman spectra are shown in Fig. 4(a) and the difference between undifferentiated pre-osteoclasts and osteoclasts at days 2, 4, and 6 are shown in Figs. 4(c) and 4(d). As shown in Fig. 4(d), the averaged second derivative Raman spectra showed a greater difference between days 0 and 4 (0D-4D) than that between days 0 and 2 (0D-2D), and the difference between days 0 and 6 (0D-6D) was similar to that between 0D-4D. The major spectral differences were in the peaks associated with proteins (phenylalanine at 1002 cm^{-1}, amide III at 1230-1320 cm^{-1} and amide I at 1665 cm^{-1}) and nucleic acids (U, C, and T at 778 cm^{-1}). As described above, these results suggest that the greater biochemical changes occurred at 4 days, reflecting the time required for fully mature osteoclast differentiation.

Multivariate statistical technique including PCA and LDA were applied to the Raman spectral data to discriminate four different time points during osteoclast differentiation. These multivariate statistical methods are superior to conventional univariate methods such as calculation of intensity or area of individual peaks because in multivariate techniques, multiple peaks or all Raman spectra are analyzed simultaneously [40]. PCA is a representative dimension reduction technique that generates new variables (i.e., principal components) accounting for most of the variance in the original variables by determining linear combinations [41]. Although PCA can easily illustrate the variation between samples, its usefulness in the classification of samples is limited because the principal components are computed to maximize the variance of the measurement matrix without considering sample groups. LDA is a more common method for the discrimination of sample groups. LDA also generates new variables (i.e., discriminant functions) by linear combinations of the original variables. In contrast to PCA, LDA aims to maximize the ratio of between-group and within-group variances. Thus, the first discriminant function provides the best separation between classes and the second discriminant function gives the second best separation between classes, and so on.

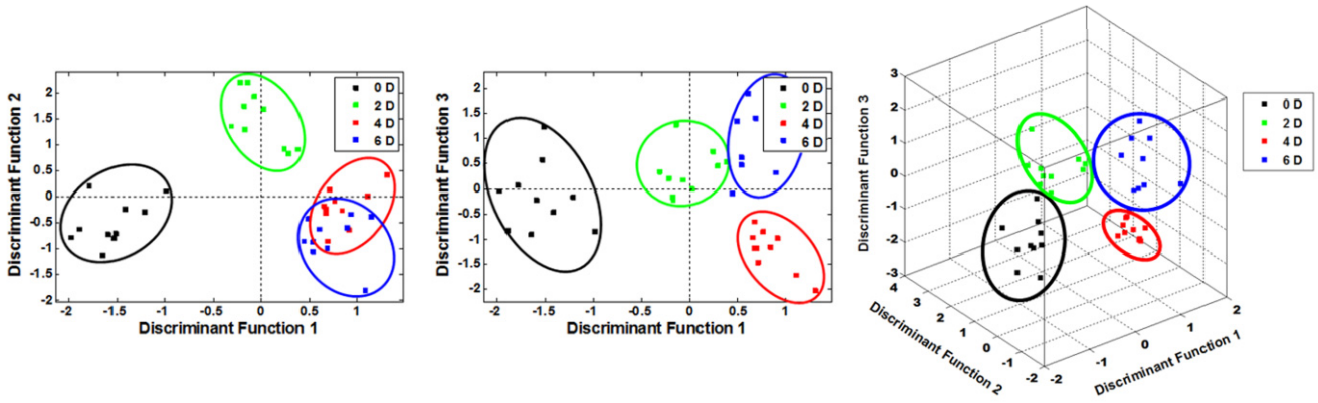

(a) (b) (c)

FIG. 5. Discriminant function (DF) scores plot: (A) DF1 vs. DF2; (B) DF1 vs. DF3; (C) DF1 vs. DF2 vs. DF3 plots for mononuclear pre-osteoclast (0 D) and differentiated cells for 2, 4 and 6 days (2 D, 4 D and 6 D).

Figure 5 shows the plots of discriminant function scores for 40 observations during a differentiation time course of osteoclastogenesis, obtained from LDA based on PCA scores. Discriminant function 1 (DF1) and discriminant function 2 (DF2) revealed a clear difference between undifferentiated pre-osteoclasts (0D) and osteoclasts at days 2 and 4 (2D and 4D) which were clustered in a very compact group and were well-separated and nonoverlapping (Fig. 5(a)). Osteoclasts at days 4 and 6 showed considerable overlap. Figure 5(b) presents the plot of DF1 versus DF3, in which the third discriminant function discriminates day 4 from day 6. Figure 5(c) shows the 3D scatter plot of discriminant function scores for all 40 observations. As shown in Fig. 5(c), the four classes were clearly separated by combining three discriminant functions. By focusing first on the difference between the four differentiation time courses for osteoclastogenesis, all-time points were clearly identified as expected based on the differences in AFM and TRAP staining, which are conventional biological assays. Combinations of the discriminant functions obtained from PCA-LDA precisely identified four classes (i.e., days 0, 2, 4, and 6). These results indicate that Raman spectroscopy combined with PCA-LDA can be used to classify osteoclast differentiation.

Raman spectroscopy with multivariate analysis can noninvasively detect biochemical markers of osteoclast differentiation, and distinguish cell status during osteoclast differentiation. The identification of unique biochemical Raman spectral signatures of cells during important cellular events, such as differentiation, may offer rapid live screening of cellular interactions.

IV. CONCLUSION

In this study, we demonstrated that Raman spectroscopy with multivariate analysis is an excellent biosensor to detect the extent of maturation during osteoclast differentiation in a non-disruptive and label free manner. Differences in mononuclear pre-osteoclasts and osteoclasts in Raman spectra are correlated with cellular events during osteoclast differentiation. High resolution AFM observation showed that transition of morphology from early to mature stages in osteoclast differentiation, which agreed with results from the conventional biological TRAP staining assay. The Raman spectroscopy results showed good agreement with AFM and the conventional biological TRAP staining assay. Therefore, Raman spectroscopy with multivariate analysis might be a useful tool for label-free and noninvasive evaluation of the maturation level of stem cell differentiation.

ACKNOWLEDGMENT

This study was supported by research fund from Chosun University 2016, the National Research Foundation (NRF) of Korea funded by the Ministry of Science (2014R1A1A 2057148 to CK), and the Ministry of Science, ICT & Future Planning (2015M3A9E2029188 to GJL).

REFERENCES

1. G. A. Rodan and T. J. Martin, "Therapeutic approaches to bone diseases," Science **289**, 1508-1514 (2000).
2. W. J. Boyle, W. S. Simonet, and D. L. Lacey, "Osteoclast differentiation and activation," Nature **423**, 337-342 (2003).
3. T. Wada, T. Nakashima, N. Hiroshi, and J. M. Penninger, "RANKL-RANK signaling in osteoclastogenesis and bone disease," Trends. Mol. Med. **12**, 17-25 (2006).
4. G. D. Roodman, K. J. Ibbotson, B. R. MacKonald, T. J. Kuehl, and G. R. Mundy, "1,25-Dihydroxyvitamin D3 causes formation of multinucleated cells with several osteoclast characteristics in cultures of primate marrow," Proc. Natl. Acad. Sci. USA. **82**, 8213-8217 (1985).
5. F. Arai, T. Miyamoto, O. Ohneda, T. Inada, T. Sudo, K. Brasel, T. Miyata, D. M. Anderson, and T. Suda, "Commitment and

differentiation of osteoclast precursor cells by the sequential expression of c-Fms and receptor activator of nuclear factor kappaB (RANK) receptors," J. Exp. Med. **190**, 1741-1754 (1999).
6. S. L. Teitelbaum, "Bone resorption by osteoclasts," Science **289**, 1504-1508 (2000).
7. B. R. Wong, R. Josien, and Y. Choi, "TRANCE is a TNF family member that regulates dendritic cell and osteoclast function," J. Leukoc. Biol. **65**, 715-724 (1999).
8. N. J. Panetta, D. M. Gupta, N. Quarto, and M. T. Longaker, "Mesenchymal cells for skeletal tissue engineering," Panminerva Medica. **51**, 25-41 (2009).
9. M. T. Cheng, H. W. Yang, T. H. Chen, and O. K. S. Lee, "Modulation of proliferation and differentiation of human anterior cruciate ligament-derived stem cells by different growth factors," Tissue Engineering Part A. **15**, 3979-3989 (2009).
10. Y. R. V. Shih, C. N. Chen, S. W. Tsai, Y. J. Wang, and O. K. Lee, "Growth of mesenchymal stem cells on electrospun type I collagen nanofibers. Stem Cells," **24**, 2391-2397 (2006).
11. J. Alock and V. Sottile, "Dynamic distribution and stem cell characteristics of Sox1-expressing cells in the cerebellar cortex," Cell Res. **19**, 1324-1333 (2009).
12. J. Lin, R. Chen, S. Feng, J. Pan, B. Li, G. Chen, S. Lin, C. Li, L. Sun, and Z. Huang, "Surface-enhanced Raman scattering spectroscopy for potential noninvasive nasopharyngeal cancer detection," J. Raman Spectrosc. **43**, 497-502 (2012).
13. M. M. Mariani, P. J. Day, and V. Deckert, "Applications of modern micro-Raman spectroscopy for cell analyses," Integr. Biol. **2**, 94-101 (2010).
14. S. Dochow, C. Kra, U. Neugebauer, T. Bocklitz, T. Henkel, G. Mayer, J. Albert, and J. Popp, "Tumour cell identification by means of Raman spectroscopy in combination with optical traps and microfluidic environments," Lab Chip. **11**, 1484-1490 (2011).
15. W. A. El-Said, T. H. Kim, H. C. Kim, and J. W. Choi, "Analysis of intracellular state based on controlled 3D nanostructures mediated surface enhanced Raman scattering," PLOS ONE **6**, e15836 (2011).
16. S. Feng, R. Chen, J. Lin, J. Pan, Y. Wu, Y. Li, J. Chen, and H. Zeng, "Gastric cancer detection based on blood plasma surface-enhanced Raman spectroscopy excited by polarized laser light," Biosens. Bioelectron. **26**, 3167-3174 (2011).
17. J. Lin, R. Chen, S. Feng, J. Pan, Y. Li, G. Chen, M. Cheng, Z. Huang, Y. Yu, and H. Zeng, "A novel blood plasma analysis technique combining membrane electrophoresis with silver nanoparticle-based SERS spectroscopy for potential applications in noninvasive cancer detection," Nanomedicine **7**, 655-663 (2011).
18. I. Notingher, J. Selvakumaran, and L. L. Hench, "New detection system for toxic agents based on continuous spectroscopic monitoring of living cells," Biosens. Bioelectron. **20**, 780-789 (2004).
19. L. L. McManus, G. A. Burke, M. M. McCafferty, P. O'Hare, M. Modreanu, A. R. Boyd, and B. J. Meenan, "Raman spectroscopic monitoring of the osteogenic differentiation of human mesenchymal stem cells," Analyst **136**, 2471-2481 (2011).
20. I. Notingher, I. Bisson, A. E. Bishop, W. L. Randle, J. M. Polak, and L. L. Hench, "In situ spectral monitoring of mRNA translation in embryonic stem cells during differentiation in vitro," Anal. Chem. **76**, 3185-3193 (2004).
21. H. G. Schulze, S. O. Konorov, N. J. Caron, J. M. Piret, M. W. Blades, and R. F. B. Turner, "Assessing differentiation status of human embryonic stem cells noninvasively using Raman microspectroscopy," Anal. Chem. **82**, 5020-5027 (2010).
22. F. C. Pascut, T. G. Huey, N. Welch, L. D. Buttery, C. Denning, and I. Notingher, "Noninvasive detection and imaging of molecular markers in live cardiomyocytes derived from human embryonic stem cells," Biophys. J. **100**, 251-259 (2011).
23. S. O. Konorov, G. Schulze, J. M. Piret, R. F. B. Turner, and M. W. Blades, "Evidence of marked glycogen variations in the characteristic Raman signatures of human embryonic stem cells," J. Raman Spectrosc. **42**, 1135-1141 (2011).
24. P. S. Hung, Y. C. Kuo, H. G. Chen, H. H. K. Chiang, and O. K. S. Lee, "Detection of osteogenic differentiation by differential mineralized matrix production in mesenchymal stromal cells by Raman spectroscopy," PLOS ONE **8**, e65438 (2013).
25. M. Xu, D. Fujita, K. Onishi, and K. Miyazawa, "Improving accuracy of sample surface topography by atomic force microscopy," J. Nanosci. Nanotechnol. **9**, 6003-6007 (2009).
26. G. J. Lee, S. Choi, J. Chon, S. Yoo, I. Cho, and H. K. Park, "Changes in collagen fibril pattern and adhesion force with collagenase-induced injury in rat Achilles tendon observed via AFM," J. Nanosci. Nanotechnol. **11**, 773-777 (2011).
27. W. A. Lam, M. J. Rosenbluth, and D. A. Fletcher, "Chemotherapy exposure increases leukemia cell stiffness," Blood **109**, 3505-3508 (2007).
28. G. Binnig, C. F. Quate, and C. Gerber, "Atomic force microscope," Phys. Rev. Lett. **56**, 930-933 (1986).
29. S. S. Schaus and E. R. Henderson, "Cell viability and probe-cell membrane interactions of XR1 glial cells imaged by atomic force microscopy," Biophys. J. **73**, 1205-1214 (1997).
30. J. K. Pijanka, K. Kumar, T. Dale, I. Yousef, G. Parkes, V. Untereiner, Y. Yang, P. Dumas, D. Collins, M. Manfait, G. D. Sockalingum, N. R. Forsyth, and J. Sule-Suso, "Vibrational spectroscopy differentiates between multipotent and pluripotent stem cells," Analyst **135**, 3126-3132 (2010).
31. E. Gazi, J. Dwyer, N. P. Lockyer, J. Miyan, P. Gardner, C. Hart, M. Brown, and N. W. Clarke, "Fixation protocols for subcellular imaging by synchrotron-based Fourier transform infrared microspectroscopy," Biopolymers **77**, 18-30 (2005).
32. A. D. Meade, F. M. Lyng, P. Knief, and H. J. Byme, "Growth substrate induced functional changes elucidated by FTIR and Raman spectroscopy in in-vitro cultured human keratinocytes," Anal. Bional. Chem. **387**, 1717-1728 (2007).
33. M. Q. Hu, J. Wang, J. Y. Cai, Y. Z. Wu, and X. P. Wang, "Analysis of sodium benzoate biotoxicity using atomic force microscope," Chin. J. Biotechnol. **24**, 1428-1432 (2008).
34. J. A. Hessler, A. Budor, K. Putchakayala, A. Mecke, D. Rieger, M. M. Banaszak Holl, B. G. Orr, A. Bielinska, J. Beals, and J. J. Baker, "Atomic force microscopy study of early morphological changes during apoptosis," Langmuir **21**, 9280-9286 (2005).
35. D. J. Taatjes, B. E. Sobel, and R. C. Budd, "Morphological and cytochemical determination of cell death by apoptosis,"

Histochem. Cell. Biol. **129**, 33-43 (2008).
36. Q. Matthews, A. Jirasek, J. Lum, X. Duan, and A. G. Brolo, "Variability in Raman spectra of single human tumor cells cultured in vitro: correlation with cell cycle and culture confluency," Appl. Spectrosc. **64**, 871-887 (2010).
37. J. W. Chan, D. S. Taylor, T. Zwerdling, S. M. Lane, K. Ihara, and T. Huser, "Micro-Raman spectroscopy detects individual neoplastic and normal hematopoietic cells," Biophys. J. **90**, 648-656 (2006).
38. G. B. Jung, Y. J. Lee, G. H. Lee, and H. K. Park, "A simple and rapid detection of tissue adhesive-induced biochemical changes in cells and DNA using Raman spectroscopy," Opt. Express **4**, 2673-2682 (2013).
39. H. M. Al-Qadin, M. Lin, M. A. Al-Holy, A. G. Cavinato, and B. A. Rasco, "Detection of sublethal thermal injury in Salmonella enterica serotype typhimurium and Listeria monocytogenes using Fourier transform infrared (FT-IR) spectroscopy (4000 to 600 cm^{-1})," J. Food. Sci. **73**, M54-61 (2008).
40. I. Notingher, G. Jell, P. L. Notingher, I. Bisson, O. Tsigkou, J. M. Polak, M. M. Stevens, and L. L. Hench, "Multivariate analysis of Raman spectra for in vitro non-invasive studies of living cells," J. Mol. Struct. **744-747**, 179-185 (2005).
41. C. M. Bishop, *Pattern Recognition and Machine Learning* (Springer, 2006).